Energetic Assessment of a High Temperature Packed Bed Storage System in Combination with a Solar Expanding-Vortex Particle Receiver

Philip Ingenhoven[1,3], Woei Saw[1,3], Muhammad Mujahid Rafique[2,3], Daniel Potter[4] (CSIRO), Alfonso Chinnici[2,3], Mehdi Jafarian[2,3], Ka Lok Lee[2,3] and G.J. 'Gus' Nathan[2,3]

[1] School of Chemical Engineering and Advanced Materials, The University of Adelaide, Adelaide (Australia)

[2] School of Mechanical Engineering, The University of Adelaide, Adelaide (Australia)

[3] Centre for Energy Technology, The University of Adelaide, Adelaide (Australia)

[4] CSIRO Energy, Newcastle, (Australia)

Abstract

A set of packed bed storage systems configured to provide high temperature air has been analyzed at around 1000°C for industrial applications, such as the calcination of alumina. In this study, a solar expanding-vortex particle receiver is selected to provide high temperature air to the storage system. The heat is then used to a drive a continuous industrial process. To ensure the uninterrupted heat supply to the process the system is hybridized with a back-up combustion heater. The main constraint of using a solar expanding vortex receiver is the management of pressure inside the receiver cavity. This is because the receiver has an open aperture, which requires a slight negative pressure to minimize particle egress as well as to maintain the stability of vortex flow inside the receiver. The complete system consists of four subsystems, namely the heliostat field, the receiver, the storage system and the process, which are simulated separately. The feasibility of such a system is explored in terms of energy shares that can be delivered by concentrated solar thermal energy. Furthermore, a preliminary techno-economic assessment is performed estimating the levelized cost of heat as well as the capacity cost of the storage system.

Keywords: high temperature, industrial process heat, solar vortex receiver, Solar Heat for Industrial Processes (SHIP), thermocline storage, hybrid energy systems

1. Introduction

Many industrial chemical processes, such as the calcination of lime and alumina, require temperatures above 1000°C. Due to the high temperature and the complexity of the various industrial processes, these belong to the class of hard to abate emissions (Bataille et al., 2018). Lime and alumina calcination use hot gas as the heat transfer medium, to which heat is presently provided by combustion of natural gas. In the context of seeking to reduce dependency on natural gas, it is desirable to use renewable energy to heat air to sufficiently high temperatures above 1000°C and displace some of the combustion processes. With current commercial solar thermal technology, as used for electricity production in solar tower systems, these temperatures are not achievable due to thermo-chemical limitations of the heat transport fluids, typically being thermal oils or molten salts (Reddy, 2011) (Zarza Moya, 2017). To reach these high temperatures, there are four classes of novel particle receiver concepts under development: the centrifugal drum receiver (Ebert et al., 2019), the falling particle curtain receiver (Ho et al., 2014), the solar expanding-vortex particle receiver (SEVR) (Chinnici et al., 2017) and the fluidized bed linear particle solar receiver (Tregambi et al., 2019). The first two concepts collect the heat exclusively in the particles, whereas in the latter two concepts are a combined medium of a carrier gas laden with particles. All four concepts have shown the potential to reach high temperatures and are also potentially configurable as air heaters. However,

Selection and/or peer review under responsibility of Scientific Committee
doi:10.18086/swc.2021.33.03 Available at http://proceedings.ises.org

the components, controls and systems needed to achieve this is different for each case and little information is available regarding how to integrate such systems into an industrial process (Kumar et al., 2019), or how to achieve effective storage of the heat (Gasia et al., 2017).
In this paper we analyze the potential of using a SEVR combined with a set of thermocline storage devices to feed hot air to an alumina calciner. The main focus of this paper is the description and analysis of the storage system. The energetic and economic performance of the complete system, as well as that of the storage system, are modelled and discussed. Solar thermal systems are highly complex and involve multiple components of different cost. It is impossible to optimize these without a system-level, techno-economic model. The aim of the paper is to demonstrate such a model for a reference configuration. The system is not yet optimal, indeed the model will be used to perform such optimizations in the future.

2. Method

2.1 Description of the system

Fig 1 presents the complete system. It consists of four subsystems that are modelled individually, namely the heliostat field, the solar receiver, the storage system and the process. The heliostat field is indicated by the sun symbol, feeding into the receiver, including a system to separate the hot air from the particles. These two systems are referred to as the concentrating solar thermal system (CST). The receiver in turn, feeds hot air into the storage system. The storage system consist of a set of thermocline devices. From the storage system hot air is fed via a backup heater into the process. In this study the subsystems were designed and modelled separately and are described in the following.

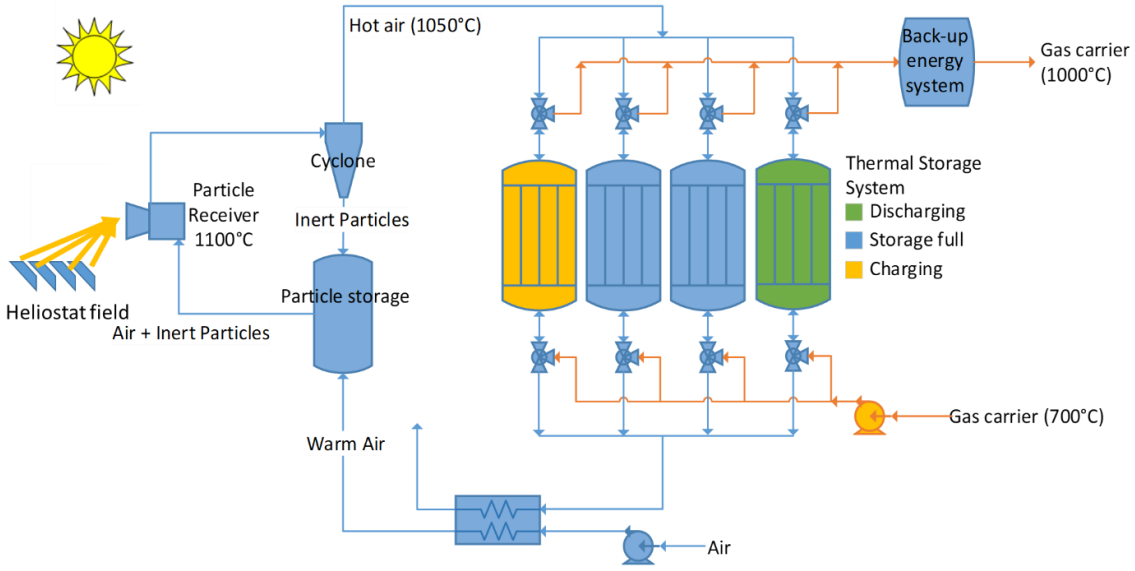

Fig 1 The system consists of a heliostat field, the solar expanding vortex receiver, including a system to separate the particulate and gaseous phase of the heat transfer medium, a set of storage devices and a backup system leading to the calcination process.

The heliostat field subsystem was modelled using Heliosim (Potter et al., 2018). Weather data from Western Australia was used to design the optimal heliostat field layout and tower height for a SEVR with nominal thermal capacity of 50MW and aperture radius of 2.75m. Tower heights between 60 and 120m were considered, and preliminary levelized cost of heat (LCOH) values for the solar concentration system were computed using a simple cost model independent from the complete system. The 5 parameters describing the radially staggered heliostat field layout (see Figure3a) were optimized using COBYLA from the NLOpt library (Johnson, 2021) where the objective function is annual optical efficiency. The optimized solar concentration system configuration with a tower height of 80m is shown in Fig 2 and Fig 3. The annual time series of solar power through the aperture for this configuration was calculated using radial basis function interpolation between a set of annually-representative sun positions. This annual time series is then fed as an input into the receiver model.

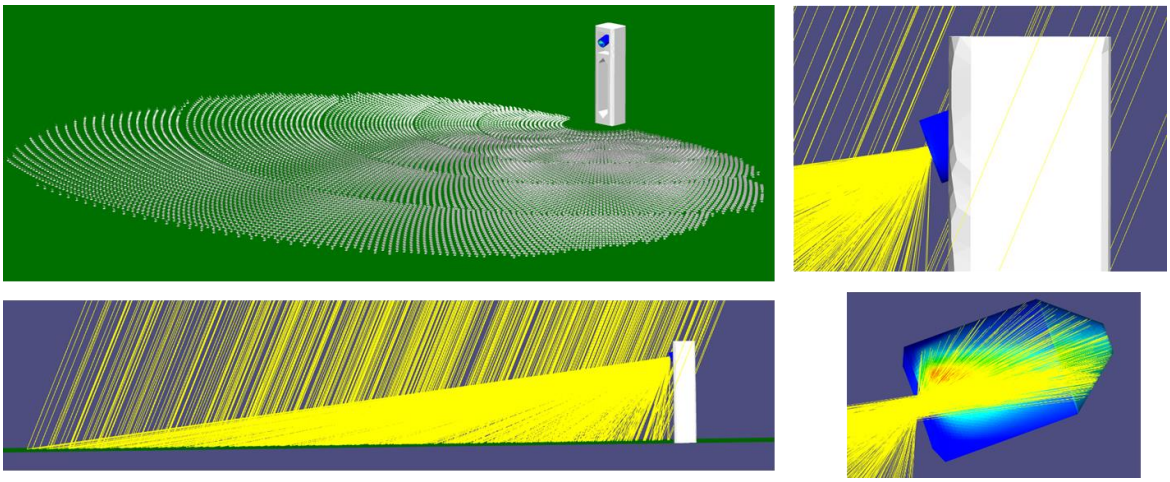

Fig 2 Visualization of the optimized heliostat field layout, tower height (80m) and SEVR geometry using Heliosim (Potter et al., 2018)

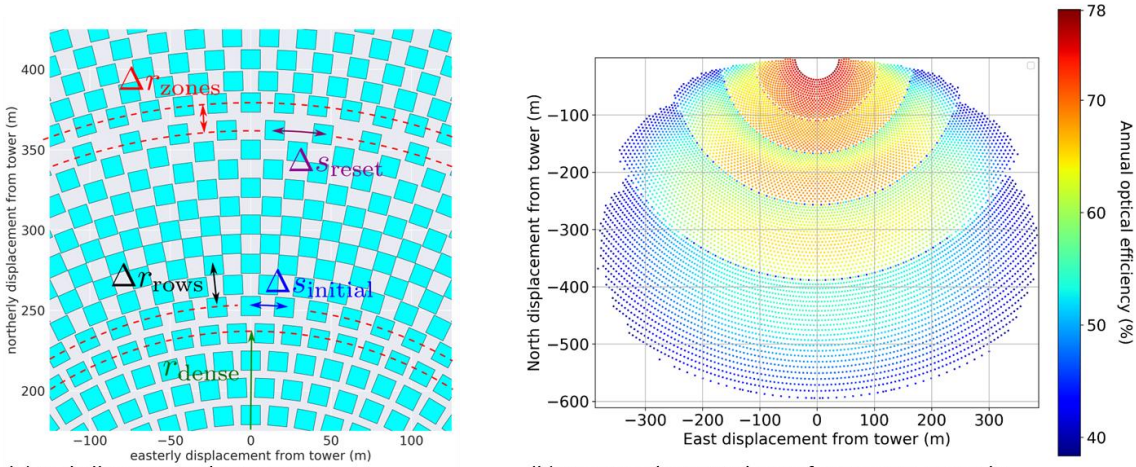

(a) Radially staggered parameters

(b) Optimised 50MW design for Western Australia (h_t=80m, r_a=2.75m)

Fig 3 Radially staggered heliostat field layout optimized using Heliosim (Potter et al., 2018)

The SEVR is a type of direct air receiver in which an air vortex within the receiver cavity is established. Air with particles in suspension enters the cavity in a conical entry and travels through the vortex to the opposite end of the cavity where it leaves the receiver through a radial exit near an open aperture (Chinnici et al., 2015). The behaviour of the SEVR is modelled using a zero-dimensional transient model (Rafique et al., 2021). The energy flows through the cavity are modelled, where the particle and gas phases, thermal losses and heat transfer between the different phases and the cavity are considered. The following assumptions and simplifications were employed:

- The solar optical input is considered to be uniformly in the cavity.
- The particles and air are uniformly distributed in the cavity.
- Gas and particles flow through the cavity with minimal recirculation
- Particles all have equal size and follow the gas flow
- Solar radiation is only absorbed by the particles and the refractory lining.

The governing equation for the model reads:

$$\dot{Q}_{sol,ap-w} = \dot{Q}_{thermal} + \dot{Q}_{rad,p-w} + \dot{Q}_{conv,w-a} + \dot{Q}_{cond,w-s} + \dot{Q}_{conv,w-s} + \dot{Q}_{re-rad,w-s}, \quad \text{(eq. 1)}$$

where $\dot{Q}_{sol,ap-w}$ is the optical heat input through the aperture to the inside surface of the cavity walls, $\dot{Q}_{thermal}$ is the heat change of receiver cavity walls, $\dot{Q}_{rad,p-w}$ is the radiative heat exchange between cavity walls and particle phase, $\dot{Q}_{conv,w-a}$ is the convective heat exchange between cavity walls and the air, $\dot{Q}_{cond,w-s}$, $\dot{Q}_{conv,w-s}$ and $\dot{Q}_{re-rad,w-s}$ are the conductive, convective re-radiative heat loss to the surroundings. Fig 4 presents the receiver cavity and the different heat flux components in the receiver cavity. The air particle mixture is fed into a system of cyclones which separates the particles from the air, only the air is then fed to the storage system and the particles are recycled into the receiver.

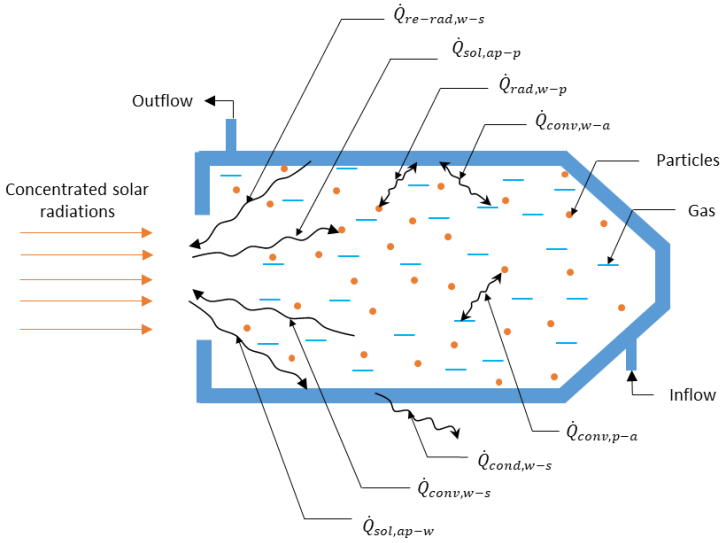

Fig 4 Schematic view of the solar expanding vortex particle receiver with all heat transfer mechanism considered in the model, where $\dot{Q}_{sol,ap-w}$ is the optical heat input through the aperture to the inside surface of the cavity walls, $\dot{Q}_{thermal}$ is the heat change of receiver cavity walls, $\dot{Q}_{rad,p-w}$ is the radiative heat exchange between cavity walls and particle phase, $\dot{Q}_{conv,w-a}$ is the convective heat exchange between cavity walls and the air, $\dot{Q}_{cond,w-s}$, $\dot{Q}_{conv,w-s}$ and $\dot{Q}_{re-rad,w-s}$ are the conductive, convective re-radiative heat losses to the surroundings.

The reaction in the alumina calcination process is the conversion of gibbsite (aluminum hydroxide) into smelter grade alumina in two steps, see equations (eq. 2) and (eq. 3).

$$2Al(OH)_3 \rightarrow 2\,AlOOH + 2H_2O \qquad \left(\Delta H_1 = 1.08\ MJ/\ kg_{Al_2O_3}\right), \qquad \text{(eq. 2)}$$

$$2AlOOH \rightarrow Al_2O_3 + H_2O \qquad \left(\Delta H_2 = 0.73\ MJ\ /\ kg_{Al_2O_3}\right), \qquad \text{(eq. 3)}$$

where ΔH_1 and ΔH_2 are the reaction enthalpies for the two reactions. As the process is about 60% efficient the total specific energy per produced kilogram of alumina amounts to 3 $MJ/\ kg_{Al_2O_3}$. The calcination of alumina takes place at 950°C in the current process. The heat from the solar system is fed into the process in the air preheater, which limits the energy share that can be provided to the whole process. Detailed questions regarding the process and the process integration are not discussed in this paper. The process is instead simplified as a heat sink with a constant heat duty with a temperature demand of 1000°C and a return temperature of 700°C. If the heat from the storage system is not sufficient to drive the process, a backup system is assumed to provide the missing part. As the optimization of the heliostat field is numerically expensive it was decided to vary the heat demand of the process between 20MW_{th} and 25MW_{th} to simulate different solar multiples. A full optimization is not possible at this stage but an optimal reference system can be chosen from the simulated configurations

2.2 The storage system model

The storage system consists of a set of thermocline storage devices, as shown in Fig 5. Each device consists of an insulated cylinder containing the storage medium. The storage is charged using hot air from the receiver as the heat transport medium. The storage medium is a packed bed of alumina balls, which is enclosed by a layer of fire bricks. Further ceramic fibers are applied as insulation, and a concrete wall encapsulates the whole system. A similar system for particle storage was proposed previously (Ma et al., 2020). The dimension of the different parts

of the containing wall used in the system are summarized in Tab 1. The height H of the storage will be optimized to find the largest solar share for each of the process sizes considered.

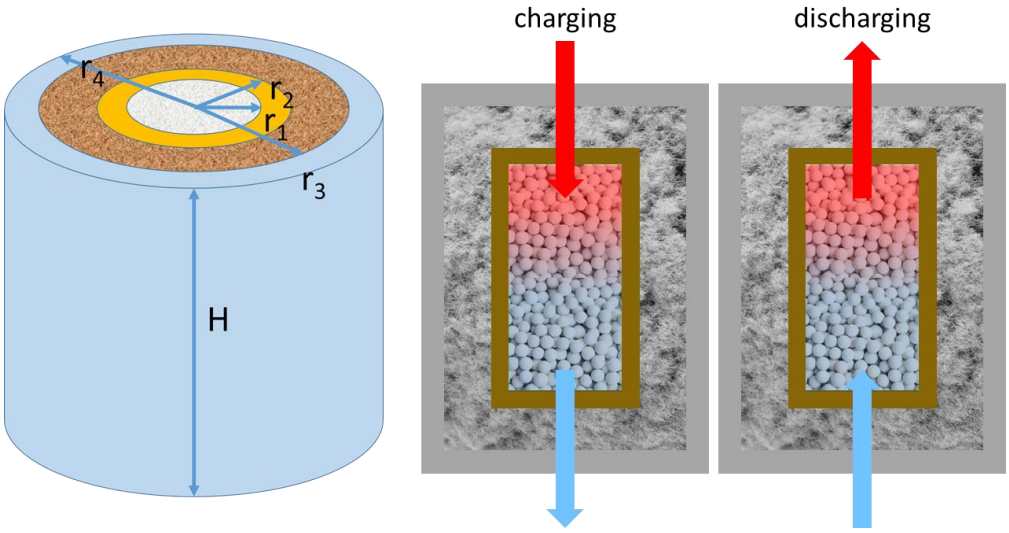

Fig 5: The storage medium is a packed bed of alumina balls, which is enclosed by a layer of fire bricks. Further ceramic fibers are applied as insulation and a concrete wall encapsulates the whole system. Radii are given in Tab 1.

Tab 1: Dimension of a single storage device consisting of the storage medium and the insulation materials

Material	Radius
Alumina spheres (storage medium)	r_1 = 2.5m
Fire brick insulation material)	r_2 = 2.8m
Ceramic fibre insulation material)	r_3 = 4.8m
Concrete (outer shell)	r_4 = 5.1m

The model used to describe the storage system is a simplified one dimensional, one phase model. It is computationally sufficiently efficient to allow fast calculation of yearly performance and still captures the most important physical properties of the storage device, namely the movement of the thermocline zone during charging and discharging. The model is described in detail previously (Hoffmann et al., 2016). The partial differential equation at the core of the model reads

$$(\rho C_p)_{eff}\,\frac{\partial T}{\partial t} + \varepsilon(\rho C_p)_{HTF} u\,\frac{\partial T}{\partial x} = k_{eff}\frac{\partial^2 T}{\partial x^2} + U_{tot}\frac{A}{V}(T - T_{ext}), \qquad \text{(eq. 4)}$$

where the heat capacities are given as $(\rho C_p)_{eff} = \varepsilon(\rho C_p)_{HTF} + (1-\varepsilon)\left(\rho C_p\right)_{stor}$, with ε=0.4 being the mean void fraction for spherical particles (Benyahia and O'Neill, 2005) in a packed bed. The heat conductivity is computed as $k_{eff} = \varepsilon k_{HTF} + (1-\varepsilon)k_{stor}$, and u being the fluid velocity. It is assumed that the temperature T is the same for the storage medium and the heat transfer fluid (HTF), this assumption is discussed and verified in (Hoffmann et al., 2016). The heat loss to the environment is described with the parameter U_{tot} and is computed using the wall parameters describes in Tab 1.

To validate the model for a single storage tank experimental data from literature was used (Meier et al., 1991). The key dimensions of the experimental setup are: diameter = 0.15 m, storage height = 1.2 m , mass flow rate = 0.004 kg/s, porosity = 0.36 and the operating temperatures T_{low} = 21°C and T_{high} =550°C. The storage temperature was measured at 7 positions along in the centre of the device along the axis of the cylinder. The results of the simulation validation is shown in Fig 6, and indicate a good agreement between model and experimental data.

The complete storage system consists of a set of thermocline storage devices, that are each described by the model defined in equation (eq. 4).

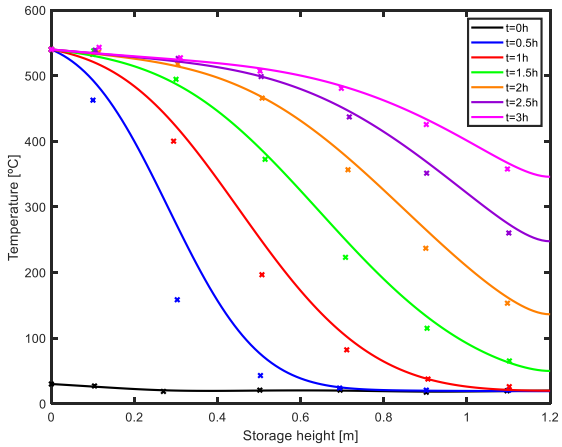

Fig 6 Simulated (solid lines) results for the thermocline storage device compared with the experimental (x) data taken from Meier et al. (1991)

2.3 The complete system model and operating strategy

To ensure the stability of the particle air vortex and to reduce particle egress through the aperture it is essential to keep the pressure and velocity within the SEVR constant. To assure this the system consists of two separate cycles, namely a charging and a discharging cycle, see Fig 1. In the charging cycle, the hot air from the receiver is fed into the storage system at a constant flow rate, to keep the receiver within constant operating parameters. Once one of the tanks is fully charged it will be switched to the discharge mode to supply heat to the process. Maintaining the charging and discharging cycles separately to allow independently manage the pressure in the receiver. To control all storage devices the temperatures at the top (inlet during charging / outlet during discharge) and at the bottom (outlet during charging / inlet during discharge) need to be measured in both the model and the real system. The operating strategy was chosen to be temperature based and will be optimized in future work. An empty or half empty storage device receives hot air from the receiver as soon as the air temperature is above the low storage set point. Then, it is charged until the temperature of the bottom of the tank reaches the charging set point. When one device is full it starts to be discharged and the next device will receive power from the solar system.

3. Results

3.1. Energetic performance

The simulation was performed for two different values of solar multiple, 2 and 2.5. The solar multiple is defined as the ratio between nominal optical solar input power and process heat demand. As the computation of different solar fields and their output for every time step is time intensive it, was decided to change the process demand instead. For a nominal optical solar input of 50MW the process heat demand was set to 25MW_{th} and 20MW_{th} respectively. Solar data was used from a location in Western Australia. The air flow through the receiver was fixed at 70.8kg/s, with a particle mass loading ratio of 10%, to reach a receiver temperature of 1100°C for nominal conditions. The process return temperature was set at 700°C. Preliminary results to visualise the storage behaviour, are shown in Fig 7 and Fig 8. Here, a system with a solar multiple of two, consisting of two storage devices with height of 13 meter (2 x 80.8MWh), was used to demonstrate the effect of the control strategy. The state of charge for the two active devices is shown in Fig 8. The fact that the state of charge is below zero at times is due to the heat losses during empty idling. The device is considered empty at 700°C. At such high temperatures the losses to the environment are not trivial.

Interestingly, in all performed simulations only two storage devices were required. To test this behaviour a set of yearly simulations were performed, with the results that the third storage device was never charged, independently from the size of the storage devices, due to the charging strategy allowing to recharge half empty devices, as long as another device can feed the process.

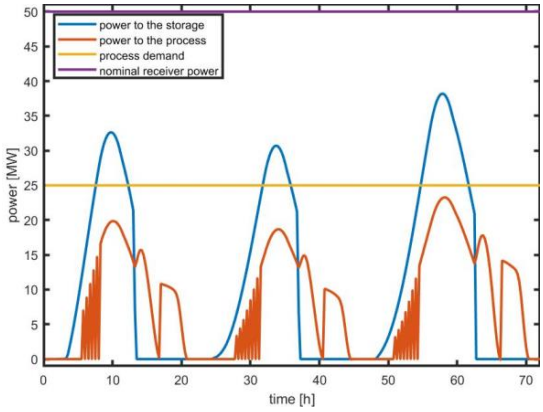

Fig 7: Power flow in the system with a solar multiple of 2, the blue line denotes the power flow from the receiver to the storage system, the red line shows the discharge from the storage system into the process, the yellow line shows the process demand, whereas the purple line shows the nominal receiver power.

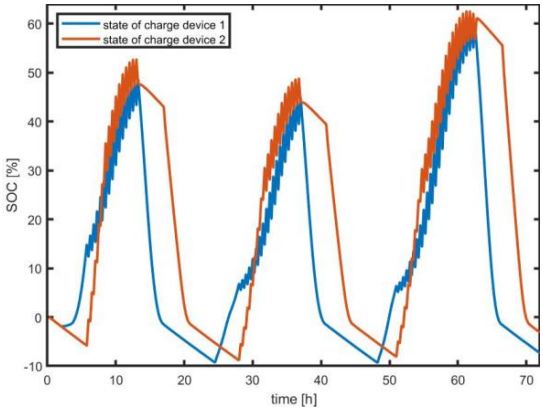

Fig 8 State of charge of the two utilized storage devices, the recharging of half full devices causes the switching between the two devices and causes fluctuations in the system

To assess an energetically optimal storage size, 14 days in summer were used to test 10 different storage device sizes (from 18.6MWh to 130.6 MWh in equidistance steps). The system consists of two storage devices. The solar share is defined as the ratio of energy delivered to the process and the process demand over a given period. The simulated solar share over the 14 day period in summer is shown in Fig 9. Interestingly the solar share rises only to certain point, after which it drops off again. This behaviour is expected, considering that the process is only ever fed from a discharging storage. Hence a very large storage device will delay the discharge and the heat has more time to be lost in the storage. For a solar multiple of two a maximal solar share of 38.8% was reached for two storage devices of 82.8MWh each, which translates to a storage height of 13.3 m for each device in the test period. For a solar multiple of 2.5, the maximal solar share in the test period is 44.0%, for a device nominal capacity of 90.4MWh and a storage height for each device of 14.5m.

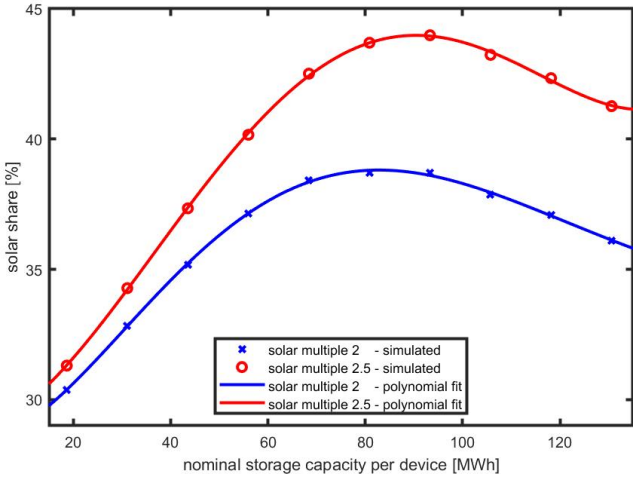

Fig 9: Solar share as a function storage size of each device. Two devices were active during the simulated time frame.

After the optimization of the storage device size, the two systems were simulated for a whole year and the results are shown in Tab 2. All the energy produced by the CST system is fed into the storage without energy spillage. The average annual heliostat field efficiency was found to be 53.6% and the average annual receiver efficiency was 73.4% in both cases. Interestingly, the increase of the solar multiple from 2 to 2.5 does not significantly influence the solar share and results in 29.4% to 33.2% solar share. The total energy delivered to the system even decreases from 64.4GWh to 58.2 GWh. This is due to the fact that a smaller process will cause the discharging to take longer and will in turn cause greater losses. This can be seen in the drop in efficiency of the storage devices for the larger solar multiple. A more detailed study analysing more values of the solar multiple would provide information on the solar multiple with the largest solar share.

Tab 2 Energetic results of the reference system for two different solar multiples for a location in Western Australia

solar multiple	SM=2	SM=2.5
process heat duty	25 MW	20 MW
total solar energy harvested:	79.8 GWh	79.8 GWh
total energy demand of the process	219 GWh	175.2 GWh
total energy into storage	79.8 GWh	79.8 GWh
total energy to process:	64.4 GWh	58.2 GWh
efficiency of storage	80.7 %	73.0 %
solar share	29.4 %	33.2 %
nominal capacity per device	82.7 MWh or 3.3 h	90.2 MWh or 4.5h
total storage time	6.6 h	9 h

3.2. Economic performance

The technical and energetic assessment presented in Section 3.1 was used to analyse the economic performance of the systems described. To understand the levelized cost of heat (LCOH) delivered to the process, it is vital to know the storage cost. The component costs were researched via market and literature research. Costs that could not be easily researched in the market were scaled to the appropriate size from Strasser and Selvam, (2014) using the scaling formula:

$$C_1 = C_2 \left(\frac{S_1}{S_2}\right)^{0.65}, \quad (5)$$

where $C_i$denotes the cost of a system with size S_i. The cost of the different subsystems is summarized in Tab 3. The levelized cost is also shown and computed using

$$LCOH = \frac{f \cdot C + O}{E}, \quad (6)$$

where C is the capital cost O is the operational cost and E is the yearly energy yield and f is the annuity factor

$$f = \frac{d(1+d)^n}{(1+d)^n - 1}, \quad (7)$$

with the discount rate d and the life time in years n.

Tab 3 summary of the economic analysis, showing the cost of the installed components and operational cost as well as the LCOH and the capacity cost.

solar multiple	SM=2	SM=2.5
capacity cost (nominal capacity)	49.9 AUD/kWh (82.7MWh)	48.9 AUD/kWh (90.2MWh)
total storage cost	AUD 8.3 million	AUD 8.8 million
process connection	AUD 8.6 million	AUD 8.6 million
CST system (heliostat field + receiver)	AUD 46.2 million	AUD 46.2 million
installed cost, entire system	AUD 63.1 million	AUD 63.9 million
OPEX	AUD 2.4 million	AUD 2.4 million
LCOH	168.8 AUD/MWh	188.3 AUD/MWh

The storage capacity cost is found to be AUD 49.9/kWh and AUD 48.9/kWh for the SM=2 and 2.5, respectively. Due to the weight of the storage, the main cost driver of the storage system are the foundations, making up 18.3% of the total storage system costs, followed by the storage material contributing 17.6% and the insulation, contributing 17.2% to the total storage systems cost. The cost of the storage system is approximately 1/8th of the total of the CST system, where the cost of the heliostat field is the main driver contributing 30.8% to the CST cost, followed by the cost for the tower contributing 25.3% of the CST cost. The LCOH is found to be 168.8 and

188.3 AUD/MWh, respectively. This is comparable to the LCOH of a DLR centrifugal receiver in between 162 and 197.6 AUD/MWh (Lubkoll et al., 2018).

3.3. Conclusions

A system model has been demonstrated that incorporates a detailed model for packed bed storage system. Due to the open aperture of the receiver it is not possible to directly feed the process with hot air. To be able to carefully manage the pressure in tat receiver, all the heat needs to go into the storage before it can be relayed to the process. In this study, no energy spillage was found and the storage round trip efficiency was found to be between 70-80%. The overall solar share can be improved if the energy can be utilized in the process directly, without going through the storage, and only storing the excess energy. This however needs changes in the receiver configuration. The low influence of the solar multiple on the solar share is concerning when larger shares of the energy need to be provided by the solar thermal system

The main driver of the LCOH is the CST system and further optimization is necessary. However, significant reductions in LCOH are expected. The current model will be further improved and used for a full optimization in future work.

Compared to the Australian hydrogen target of 2 AUD/kg, which is equivalent to 60 AUD/MWh, the solar thermal reference solution analysed in this study is about 3 times more expensive. Current levelized cost of electricity from wind and solar are between 36 and 72 AUD/MWh (“Levelized Cost of Energy and of Storage,” n.d.). The best case in this study achieves a LCOH of 168.8 AUB/MWh, providing only 29.4% of the yearly process energy demand. This is at least twice as costly as using electricity from solar and wind, which can provide higher renewable shares in combination, even without storage, in some locations. The analysed storage in this study has a very low capacity cost of just under 50AUD/kWh and is more economical than electro-chemical storage systems such as batteries. Thus, the combination of renewable electricity and thermal storage is an interesting option worth investigating.

The problem of decarbonizing high temperature industrial processes is far from being solved and much future investigation into all available technologies, such as solar thermal, hydrogen and electrification has to be done. Further exploration of new chemical production routes to reduce the temperature demand is also necessary to tackle this challenge.

4. Acknowledgments

This project received funding from ARENA through grant 2015/RND054 as part of ARENA's Research and Development Programme.

5. References

Bataille, C., Åhman, M., Neuhoff, K., Nilsson, L.J., Fischedick, M., Lechtenböhmer, S., Solano-Rodriquez, B., Denis-Ryan, A., Stiebert, S., Waisman, H., Sartor, O., Rahbar, S., 2018. A review of technology and policy deep decarbonization pathway options for making energy-intensive industry production consistent with the Paris Agreement. J. Clean. Prod. 187, 960–973. https://doi.org/10.1016/j.jclepro.2018.03.107

Benyahia, F., O’Neill, K.E., 2005. Enhanced Voidage Correlations for Packed Beds of Various Particle Shapes and Sizes. Part. Sci. Technol. 23, 169–177. https://doi.org/10.1080/02726350590922242

Chinnici, A., Arjomandi, M., Tian, Z.F., Lu, Z., Nathan, G.J., 2015. A Novel Solar Expanding-Vortex Particle Reactor: Influence of Vortex Structure on Particle Residence Times and Trajectories. Sol. Energy 122, 58–75. https://doi.org/10.1016/j.solener.2015.08.017

Chinnici, A., Xue, Y., Lau, T.C.W., Arjomandi, M., Nathan, G.J., 2017. Experimental and numerical investigation of the flow characteristics within a Solar Expanding-Vortex Particle Receiver-Reactor. Sol. Energy 141, 25–37. https://doi.org/10.1016/j.solener.2016.11.020

Ebert, M., Amsbeck, L., Rheinländer, J., Schlögl-Knothe, B., Schmitz, S., Sibum, M., Uhlig, R., Buck, R., 2019. Operational experience of a centrifugal particle receiver prototype. AIP Conf. Proc. 2126, 030018. https://doi.org/10.1063/1.5117530

Gasia, J., Miró, L., Cabeza, L.F., 2017. Review on system and materials requirements for high temperature thermal energy storage. Part 1: General requirements. Renew. Sustain. Energy Rev. 75, 1320–1338. https://doi.org/10.1016/j.rser.2016.11.119

Ho, C., Christian, J., Gill, D., Moya, A., Jeter, S., Abdel-Khalik, S., Sadowski, D., Siegel, N., Al-Ansary, H., Amsbeck, L., Gobereit, B., Buck, R., 2014. Technology Advancements for Next Generation Falling Particle Receivers. Energy Procedia, Proceedings of the SolarPACES 2013 International Conference 49, 398–407. https://doi.org/10.1016/j.egypro.2014.03.043

Hoffmann, J.-F., Fasquelle, T., Goetz, V., Py, X., 2016. A thermocline thermal energy storage system with filler materials for concentrated solar power plants: Experimental data and numerical model sensitivity to different experimental tank scales. Appl. Therm. Eng. 100, 753–761. https://doi.org/10.1016/j.applthermaleng.2016.01.110

Johnson, S.G., 2021. The NLopt nonlinear-optimization package [WWW Document]. URL http://ab-initio.mit.edu/nlopt (accessed 10.6.21).

Kumar, L., Hasanuzzaman, M., Rahim, N.A., 2019. Global advancement of solar thermal energy technologies for industrial process heat and its future prospects: A review. Energy Convers. Manag. 195, 885–908. https://doi.org/10.1016/j.enconman.2019.05.081

Levelized Cost of Energy and of Storage [WWW Document], n.d. . Lazard.com. URL http://www.lazard.com/perspective/levelized-cost-of-energy-levelized-cost-of-storage-and-levelized-cost-of-hydrogen/ (accessed 10.15.21).

Lubkoll, M., Harms, T., von Backström, T., Amsbeck, L., Buck, R., Hockaday, S., 2018. (16) (PDF) Integrating Solar Process Heat into Manganese Ore Pre-heating. Presented at the 5th Southern African Solar Energy Conference, Durban, South Africa.

Ma, Z., Davenport, P., Zhang, R., 2020. Design analysis of a particle-based thermal energy storage system for concentrating solar power or grid energy storage. J. Energy Storage 29, 101382. https://doi.org/10.1016/j.est.2020.101382

Meier, A., Winkler, C., Wuillemin, D., 1991. Experiment for modelling high temperature rock bed storage. Sol. Energy Mater. 24, 255–264. https://doi.org/10.1016/0165-1633(91)90066-T

Potter, D., Kim, J.-S., Khassapov, A., Pascual, R., Hetherton, L., Zhang, Z., 2018. Heliosim: An Integrated Model for the Optimisation and Simulation of Central Receiver CSP Facilities. https://doi.org/10.1063/1.5067213

Rafique, M.M., Nathan, G., Saw, W., 2021. A mathematical model to assess the influence of transients on a refractory-lined solar receiver. Renew. Energy 167, 217–235. https://doi.org/10.1016/j.renene.2020.11.077

Reddy, R.G., 2011. Molten Salts: Thermal Energy Storage and Heat Transfer Media. J. Phase Equilibria Diffus. 32, 269. https://doi.org/10.1007/s11669-011-9904-z

Strasser, M.N., Selvam, R.P., 2014. A cost and performance comparison of packed bed and structured thermocline thermal energy storage systems. Sol. Energy 108, 390–402. https://doi.org/10.1016/j.solener.2014.07.023

Tregambi, C., Bevilacqua, C., Cammarota, A., Chirone, R., Salatino, P., Solimene, R., Bassetti, F., Picarelli, A., Magaldi, M., 2019. Experimental characterization of granular materials for directly irradiated fluidized bed solar receivers. AIP Conf. Proc. 2126, 030060. https://doi.org/10.1063/1.5117572

Zarza Moya, E., 2017. 5 - Innovative working fluids for parabolic trough collectors, in: Blanco, M.J., Santigosa, L.R. (Eds.), Advances in Concentrating Solar Thermal Research and Technology, Woodhead Publishing Series in Energy. Woodhead Publishing, pp. 75–106. https://doi.org/10.1016/B978-0-08-100516-3.00005-8